

A vector intensity-based equivalent wavepacket model for high-performance military aircraft jet noise

Eric B. Whiting, Kent L. Gee, Trevor A. Stout, Tracianne B. Neilsen, Alan T. Wall, and Michael M. James

Citation: *Proc. Mtgs. Acoust.* **25**, 045007 (2015); doi: 10.1121/2.0001236

View online: <https://doi.org/10.1121/2.0001236>

View Table of Contents: <https://asa.scitation.org/toc/pma/25/1>

Published by the [Acoustical Society of America](#)

ARTICLES YOU MAY BE INTERESTED IN

[Techniques for the rapid calculation of the excitation pattern in the time varying extensions to ANSI S3.4-2007](#)
Proceedings of Meetings on Acoustics **36**, 040002 (2019); <https://doi.org/10.1121/2.0001206>

[National occupational research agenda for Hearing Loss Prevention](#)
Proceedings of Meetings on Acoustics **36**, 040003 (2019); <https://doi.org/10.1121/2.0001218>

[Design and realisation of a directional electric vehicle warning sound system](#)
Proceedings of Meetings on Acoustics **39**, 040001 (2019); <https://doi.org/10.1121/2.0001224>

[Laboratory simulations of conversation scenarios: questionnaire results from patient and partner](#)
Proceedings of Meetings on Acoustics **39**, 050004 (2019); <https://doi.org/10.1121/2.0001245>

[Application of autoencoder to traffic noise analysis](#)
Proceedings of Meetings on Acoustics **39**, 055003 (2019); <https://doi.org/10.1121/2.0001227>

[Wavenumber interactions of turbulent boundary layer flow with structures exhibiting the acoustic black hole effect](#)
Proceedings of Meetings on Acoustics **39**, 065002 (2019); <https://doi.org/10.1121/2.0001231>



POMA Proceedings
of Meetings
on Acoustics

**Turn Your ASA Presentations
and Posters into Published Papers!**



170th Meeting of the Acoustical Society of America

Jacksonville, Florida

2–6 November 2015

Physical Acoustics: Paper 4pPA6

A vector intensity-based equivalent wavepacket model for high-performance military aircraft jet noise

Eric B. Whiting

Brigham Young University, Provo, UT, 84602; benweric@gmail.com

Kent L. Gee

Department of Physics and Astronomy, Brigham Young University, Provo, UT, 84602; kentgee@byu.edu

Trevor A. Stout and Tracianne B. Neilsen

Brigham Young University, Provo, UT 84602; titorep@gmail.com; tbn@byu.edu

Alan T. Wall

Air Force Research Laboratory, Wight-Patterson Air Force Base, OH; alan.wall.4@us.af.mil

Michael M. James

Blue Ridge Research and Consulting, LLC, Asheville, NC; michael.m.james@blueridgeresearch.com

In this paper, a wavepacket ansatz is used to create an analytical model for the jet noise radiation from a high-performance military aircraft. Unlike other equivalent, acoustics-based wavepacket source models, this one is designed to match the measured acoustic vector intensity at a number of positions in the jet near field for both military power and afterburner engine conditions. The complex pressure of a line source is defined according to an analytical hyperbolic tangent wavepacket model and Rayleigh integration is used to find the pressure, particle velocity, and time-averaged intensity at observer locations. A cost function developed from the modeled and measured acoustic intensity vectors is used in a simulated annealing algorithm to find the optimal wavepacket parameters. Although this source modeling approach neglects some source characteristics, it also provides a relatively simple equivalent source modeling methodology that provides insights into tactical jet noise radiation.

1. INTRODUCTION

The impact of high-performance military aircraft noise on nearby personnel and surrounding communities is of vital concern because of the potential for hearing loss and human annoyance. In order to better predict the noise impact, modeling tools are needed that accurately predict the spatial variation of the levels, spectral content, and coherence properties of the partially correlated noise field. The turbulent mixing noise from high-power jets originates from the interaction of turbulent structures traveling along the shear layer with the ambient air.¹ Instead of modeling these complicated fluid interactions, an acoustic equivalent source model strives to obtain a representation of the noise sources that can be used to efficiently predict the sound field. An extensive set of measurements taken near a tethered advanced tactical aircraft has been analyzed in many ways²⁻⁶ with the overarching goal of creating an equivalent source model for the radiated noise. One unique set of measurements from this experiment is of acoustic vector intensity. In this paper, the measured intensity vectors are used to find an equivalent source representation of the jet noise based on an analytical wavepacket-based equivalent source.

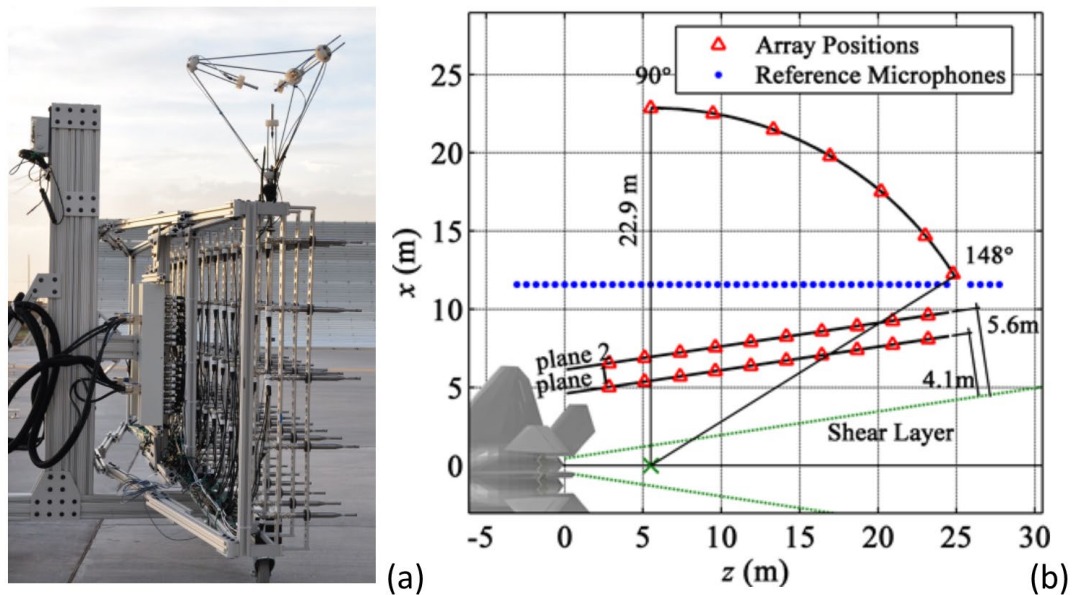


Figure 1. Experimental Setup. (a) Photograph of the intensity probe on top of the 90 microphone array. (b) Schematic of noise measurements of a tethered high-performance military aircraft. The red triangles indicate the positions of the 90 microphone array.

An extensive set of noise measurements in the vicinity of the tied-down tactical aircraft were made jointly by the Air Force Research Laboratory, Blue Ridge Research and Consulting, LLC, and Brigham Young University. A detailed description of the experiment is found in Wall *et al.*⁷ A three-dimensional intensity probe was placed on top of an array of microphones that was moved to the locations indicated by the red triangles in Fig. 1. One of the engines was sequentially operated at four engine conditions: idle, intermediate (80% ETR), military (100% ETR), and afterburner, while the other engine was held at idle.

The data set has been analyzed in multiple ways to learn about the properties of an equivalent source. The first equivalent source model of the jet noise was constructed using the levels recorded by the 90 microphone array². The underlying simple sources were two line arrays of acoustic point sources, one with a constant phase relationship to produce directional noise and the other with a random phase relationship to produce omnidirectional noise. This model matched the interference pattern seen on large planes of data. Subsequent equivalent source modeling efforts^{4,5} have been based on an analytical wavepacket representation of the jet noise.⁸ Wavepackets share characteristics with instability wave theory that has been used to model the hydrodynamic and near-field acoustic pressure fluctuations.⁹⁻¹⁴ Equivalent source wavepackets have been deduced from the decomposition of level-based, ground array measurements into contributions associated with fine and large-scale turbulent structures.¹⁵ The resulting wavepackets show a remarkable degree of self-similarity across frequency. In addition, the source distributions obtained from various phased-array methods

have been decomposed into a multiple-wavepacket representation⁴ that can be used to predict not only the levels of the sound field but also the coherence properties. This paper reports on an equivalent source wavepacket model obtained from the acoustic intensity measurements.

Acoustic intensity measurements have been utilized in a few aeroacoustics settings. One of the first uses was by Roth,¹⁶ who performed a two-microphone intensity measurement in the near and far fields of a hot and cold jets in an anechoic chamber. Then the results were verified by comparing to jet noise prediction models and by placing a speaker at the location of interest. One advantage of intensity vectors is the ability to ray trace the vector back to a source region. Jaeger and Allen¹⁷ demonstrated this with two orthogonal pairs of microphones. The acoustic intensity was found away from a Mach-0.2 to 0.6 lab-scale cold jet. Then the vectors were traced backward to the centerline of the jet. This showed a region over which the source region extended. For small sources, this capability might not be very important, but for large sources like rocket engines the source region and plume can be quite large (100 feet). It would be impractical to use an array of microphones to characterize the noise. It is advantageous to use intensity probes at a few discrete locations to characterize the noise source region for the plume.

Stout et al.¹⁸ used intensity measurements to characterize the noise radiation from the tactical aircraft. Using the (then) newly developed PAGE method for vector intensity¹⁹, the intensity at the 27 probe locations was calculated. Then, using the vectors that had a magnitude within 3 dB of the peak magnitude, the source region was found by tracing the intensity vector back to the center line of the jet. Furthermore, a numerical study was performed to show that the vectors within 3 dB of the peak magnitude originates from the region above eighty percent of the maximum energy. A further study showed that the radiated vector intensity field could be represented by analytical wavepacket-like functions.²⁰

Building on prior source characterization methods using acoustic vector intensity, this paper contains a description of how the measured intensity is used to obtain an equivalent wavepacket-based source representation of the jet noise. The analytical wavepacket model proposed by Papamoschou²¹ is used to define the amplitude and phase of the equivalent source. A simulated annealing optimization finds the frequency-dependent wavepackets that minimize the difference between the measured and modeled acoustic intensity vectors. It is shown that this single-wavepacket model predicts that the source region contracts and moves upstream as frequency increases. Limitations of using a single-wavepacket to model the entire sound intensity field are discussed.

2. METHODS

A. WAVEPACKET MODEL

A wavepacket has been described as a spatially extended source characterized by an axial amplitude distribution that grows, saturates and decays, an axial phase relationship that produces directional noise,²² and correlation lengths longer than the integral length scales of the turbulence.²³ Wavepacket characteristics are found in the turbulent region, the hydrodynamic near field and the acoustic far field.⁸ The wavepacket representation includes a spatial phase relationship across the source distribution such that the resulting sound is highly directional. Wavepacket investigations of jet noise have been conducted using measurements in the turbulent region, hydrodynamic near field, and acoustic far field of laboratory-scale jets.⁹⁻¹⁴ Wavepackets provide an opportunity to find an equivalent source model for high-power jet noise.

A wavepacket representation of jet noise has been investigated for laboratory-scale jet noise experiments. Morris¹⁴ compared the wavenumber spectrum of the measured spectral density in the far field to the pressure wavenumber spectrum on a cylinder in the near field. Similarly, Papamoschou²¹ showed that the far-field acoustic levels from a cold, lab-scale Mach 0.9 jet can be modeled as the field from a single wavepacket if a monopole was included to account for the sound radiation to the side of the engine nozzle. This work shows that a single volume velocity (source strength) wavepacket comprised of a line of monopoles can be used to model the acoustic intensity from a tethered aircraft at military and afterburner conditions.

Acoustic vector intensity can be modeled by an analytical wavepacket source model. Calculation of the acoustic intensity requires a volume velocity (or source strength) distribution defined on the jet centerline that can be used to model both the pressure and particle velocity. In practice, this is accomplished by assigning the magnitudes and phases of the source distribution to a line array of acoustic point sources on the jet centerline. For this work, the acoustic pressure at the nozzle lip-line is represented by an analytical wavepacket model that

was used by Papamoschou.²¹ Instead of representing the pressure fluctuations, this wavepacket defines the relative amplitude and phase of acoustic point sources as a function of location, z_m , and angular frequency, ω :

$$\tilde{Q}(z_m, \omega) = \tanh\left(\left(\frac{z_m}{b_1}\right)^{g_1}\right) \left(1 - \tanh\left(\left(\frac{z_m}{b_1}\right)^{g_2}\right)\right) e^{-\frac{j\omega}{U_c}z_m}, \quad (1)$$

where U_c is the convective velocity. Because the convective velocity determines the phase relationship across the point sources, it determines the frequency-dependent directionality of the sound.²⁴ This directionality best represents the Mach wave radiation from the large-scale turbulent structures. The direction of the highest sound level is θ_{peak} :

$$\cos \theta_{\text{peak}} = \frac{c}{U_c}, \quad (2)$$

where θ_{peak} is measured relative to the jet centerline, and c is the ambient sound speed in the air outside the jet. The parameters of first hyperbolic tangent term, b_1 and g_1 , control the length scale and the rate of the growth of the wavepacket amplitude, respectively. Similarly, b_2 and g_2 dictate the length scale and rate of the amplitude decay.

As examples of how the modeling parameters affect the amplitude distribution, a series of normalized wavepacket shapes is shown in Fig. 2, in which one parameter is changed in each plot, with the parameters [b_1, b_2, g_1, g_2 , and U_c] shown in the title of each plot. Decreasing the value of U_c (in Fig. 2f), does not change the shape of the envelope. However, decreasing U_c affects the phase of the sources. This alters the direction at which the main lobe radiates. Adjustments in b_1, g_1, b_2, g_2 control both the extent and rate of the wavepacket rise and decay. These five parameters are varied in a simulated annealing optimization algorithm to find equivalent source strengths that model the measured intensity.

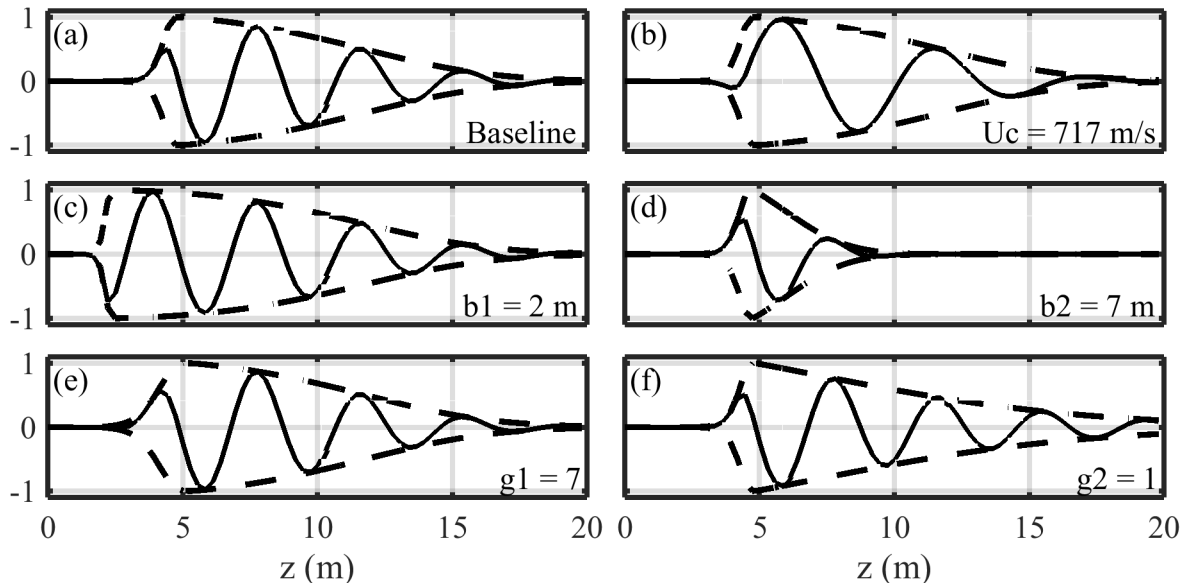


Figure 2. Various normalized wavepacket shapes. The baseline parameters are $U_c = 478$ m/s, $b_1 = 4$ m, $b_2 = 14$ m, $g_1 = 14$ m, and $g_2 = 2$ m. For the various plots (b)-(f), one parameter is changed from the baseline and is indicated in the plot.

In order to predict the acoustic intensity at the measurement locations, estimates of the total pressure and particle velocity are needed. The pressure from each point source is obtained assuming spherical spreading:

$$\tilde{p}_m(r, \omega) = \frac{j\rho_0 c k \tilde{Q} e^{-jkr_m}}{4\pi r_m}, \quad (3)$$

where r_m is the distance from the point source to the desired location, $\tilde{p}_m(r)$ is the complex pressure at the desired location, ω is the angular frequency of the source, k is the wavenumber, and \tilde{Q} is the complex volume velocity of the monopole source in Eq. (1). The linearized Euler's equation is used to get the particle velocity at the desired location, $\tilde{u}_m(r)$:

$$\tilde{u}_m(r, \omega) = \left(\frac{j}{\rho_0 \omega}\right) \nabla p_m = \frac{\tilde{Q} e^{-jkr_m} (1 + jkr_m)}{4\pi r_m^2} \hat{r}, \quad (4)$$

and \hat{r} is the unit direction from the source to the desired location.

The total contribution of all the point sources to the acoustic intensity is found by the coherent summation of the pressure and the particle velocity. The time-averaged acoustic intensity is modeled by

$$\vec{I}(\omega) = \frac{1}{2} \text{Re} \left\{ \left(\sum_m \tilde{p}_m(r, \omega) \right) \left(\sum_m \tilde{u}_m(r, \omega) \right)^* \right\}, \quad (5)$$

where $*$ indicates the complex conjugate.

This wavepacket-based model for the acoustic intensity could be modified to include the ground reflection present because the F-22 was tethered to a concrete pad. An image source could be included in the calculation of the pressure and velocity. For this study, the image source is not included because the sparseness of the intensity measurements limits the spatial information about the ground reflections, except the presence of one at ~ 500 Hz.³

B. SIMULATED ANNEALING ALGORITHM

A simulated annealing algorithm²⁵ is used to find volume velocity wavepackets that provide the best match to the measured acoustic vector intensity. The error between the measured and modeled intensity vectors is quantified with the cost function, E . The simulated annealing algorithm makes random steps in the multidimensional parameter space. The step size in each of the five wavepacket model parameters is a random number multiplied by the difference between the upper and lower bounds for that parameter. A scale factor is included that allows the algorithm to make smaller steps as the annealing progresses in order to improve convergence. The simulated annealing algorithm is designed to always accept steps that reduce the cost function (a downhill step), and with a certain probability, accept uphill steps via the Metropolis criteria²⁶ in search for the global minimum. The probability of accepting an uphill step decreases as the algorithm progresses.

The bounds on these parameters were chosen to represent a wide range of wavepacket shapes. The boundaries for the convective speed, U_c , are chosen to provide a physically realistic direction of the maximum radiation angle. The intensity measurements at the 22.9 m arc are used to find the angle associated with the peak level. Since there were seven locations on the arc, MATLAB's spline function was used to interpolate between the measurement points to identify the maximum angle. Previous studies (e.g., Ref. 27) have shown that angles close to the F-22 need to be defined not relative to the nozzle exit plane ($z = 0$), but rather 7-8 nozzle diameters downstream, shown as the "x" at $z = 5.5$ m in Fig. 1, to align with observed far-field directivity angles. Taking this difference into account, an angular range of $\pm 10^\circ$ about the peak angle is converted to a range of convective velocities using Eq. (2). This process allows for physically realistic bounds to be set on the values of U_c sampled in the simulated annealing algorithm.

Although there is not a direct tie to measurements as in the case of U_c , general physical features are used to set constraints on the remaining four parameters. Since b_1 and b_2 correspond to the length scale of the rise and fall of the source region, the upper bound on each is the length of the modeled source and the lower limit is set to 0.1λ . An additional constraint is $b_1 > b_2$, because there was little change to the wavepacket shape when $b_1 <$

b_2 . Furthermore, from previous jet noise source characterizations (e.g., see Figs. 28 and 33 in Ref. 28), it is expected that the source distribution should rise faster than it decays. This translates into the constraint that $g_1 > g_2$ for the sampled parameters.

The simulated annealing optimization seeks to maximize the agreement between the modeled and measured intensity vectors by minimizing the cost function E . Because the wavepacket amplitude was not included as a modeling parameter, all components of the measured and modeled intensity vectors were each normalized by the magnitude of the largest vector. Because of the multi-dimensional nature of the vectors, the cost function is the Euclidian distance between modeled and measured vectors. This cost function guides the simulated annealing algorithm to wavepacket modeling parameters that achieve the best agreement between the magnitude and angle of the modeled and measured intensity vectors. An example of the convergence of the simulated algorithm is shown in Fig. 3. For all trials, a minimum cost was reached in fewer than 10000 iterations. Most of the trial runs converged to the same cost, indicating convergence to an equivalent minimum.

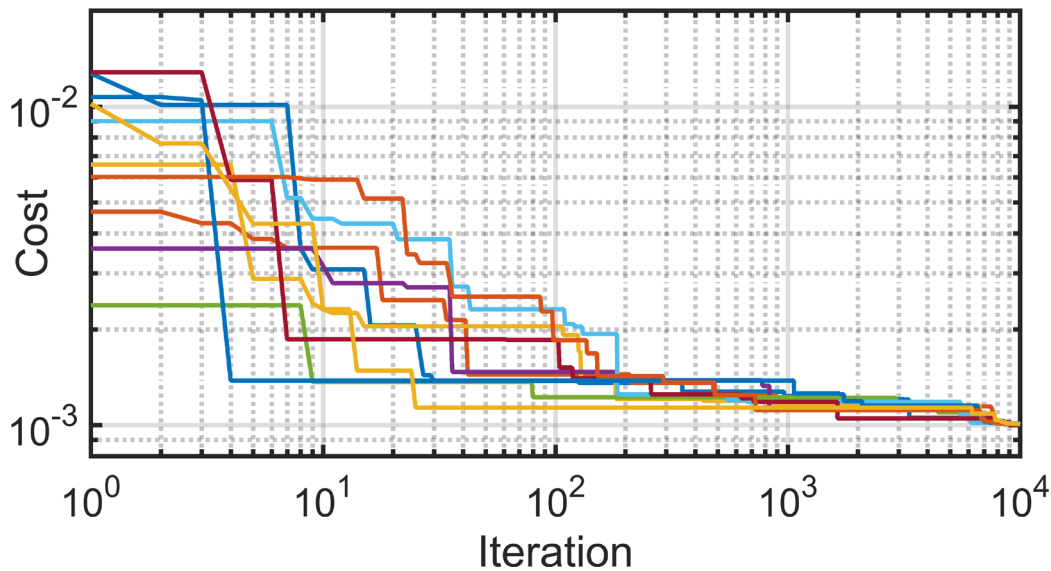


Figure 3. The various cost functions for military engine condition at 125 Hz for 10 different optimization runs.

C. OPTIMIZATION VALIDATION

In order to validate the method, the simulated annealing procedure was applied to generated intensity levels from known parameters. Instead of using the measured data, wavepacket parameters were chosen to create a new wavepacket. The pressure and particle velocity were found at each of the measurement locations. By comparing the simulated model to the results of the simulated annealing algorithm, it can be determined how well the algorithm finds the best solution. Ideally, the algorithm should exactly match, and the cost function should go to zero. But the simulated annealing algorithm is a heuristic approach, which means it does not guarantee an exact match.

After running one hundred optimizations using simulated data generated from the same wavepacket parameters, the results match well. As can be seen from Table 1, the actual values are within one standard deviation from the mean. The estimate could be improved by running more trials or removing all the results that are much greater than the lowest cost function.

Table 1. Initial and optimized wavepacket parameters for 125 Hz military condition. The top row lists the chosen parameters for the simulated wavepacket. The second and third row indicate the mean and standard deviation, respectively, after the 100 optimization runs.

	U_c (m/s)	b_1 (m)	b_2 (m)	g_1	g_2
Source Parameters	478	4.4	14.2	13	2.7
Optimized Results	478 ± 4	4.3 ± 0.2	14.1 ± 1.2	17.5 ± 6.1	2.7 ± 0.3

The validation model shows that some wavepacket parameters are more sensitive than others. The b_1 parameter has a very small standard deviation indicating that good results are only achievable with an accurate estimate of this parameter. On the other hand, the g_1 parameter has a very large standard deviation indicating that the model is not as sensitive to this parameter. Because of the accuracy of this optimization validation, the optimization procedure can find the wavepacket model that best fits the measured high-performance jet aircraft data.

Another verification method is to compare the levels and direction of the measured and modeled data. An example of the agreement is displayed in Fig. 4. The top part of the figure shows the real part and magnitude of the analytical wavepacket (defined in Eq. 1) for the modeling parameters obtained by the simulated annealing algorithm. This optimized volume velocity wavepacket is used to model the intensity, using Eq. 5, at the measurement locations shown in Fig. 1. Fig. 4 shows that the modeled and measured data match well for sound intensity level and direction of the acoustic intensity vector. The good agreement can be further seen in Fig. 5, which compares the measured acoustic intensity vectors (5a) to the modeled results (5b). As expected at this low frequency, the intensity vectors point downstream and away from the source. Besides good agreement at the measurement locations, Fig. 5b shows the intensity level elsewhere. This allows visualization of the Mach wave/large-scale structure radiation, which the wavepacket model best matches.

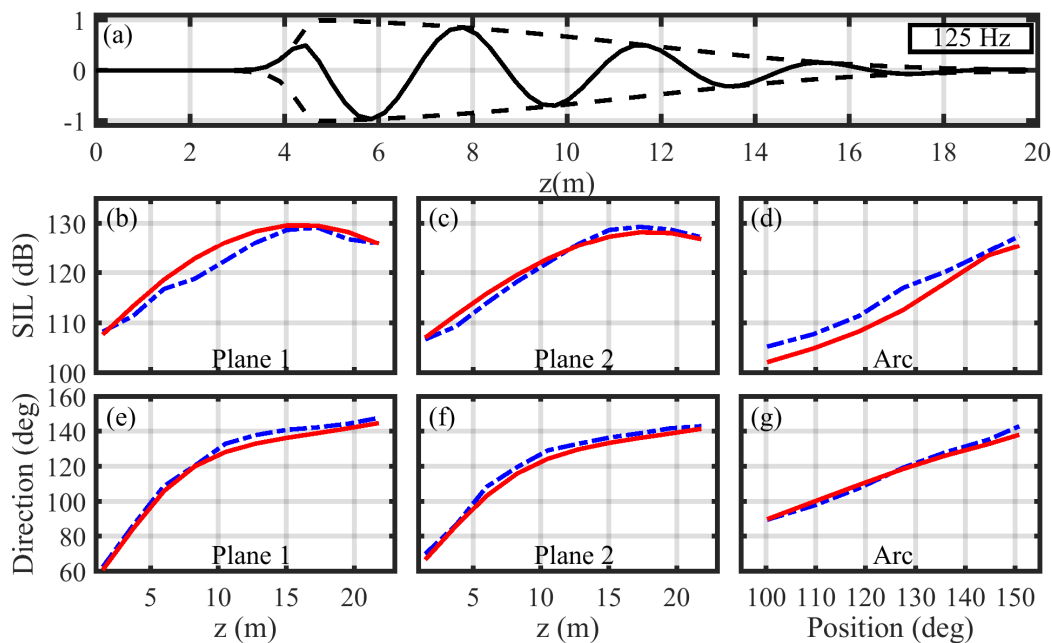


Figure 4. The wavepacket (a) that best fits the measured data for Military Engine Condition at 125 Hz. The center line shows the measured (blue dashed) and modeled (red) intensity magnitude for the three intensity probe measurement planes (b), (c), and arc (d), as in Fig. 1b. The bottom line shows the agreement of measured and modeled intensity directions for the same three probe measurement locations.

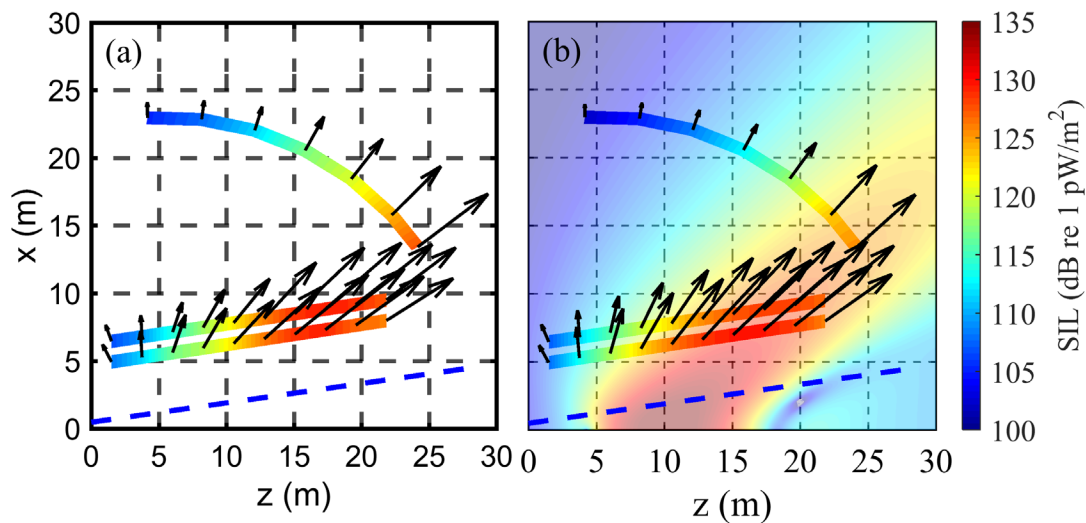


Figure 5. For 125 Hz and military engine conditions, (a) shows the measured acoustic intensity vectors, and subplot (b) shows the optimized intensity vectors. Subplot (b) also has the predicted intensity level throughout the region.

3. RESULTS

For both military and afterburner conditions, the wavepackets for one third octave bands were computed based on the measured acoustic intensity.

A. MILITARY ENGINE CONDITION

Traditional wavepacket envelope shapes have smoothly varying contours with gentle rise and fall characteristics^{4,5,21} Unlike these traditional wavepackets, this study found that the optimal wavepackets have a steep rise, which corresponds to an increase in radiation in the upstream direction. This also suggests that the typical wavepacket source found in the foundational studies is intended to match only the peak radiation direction. Most of these studies, e.g. Ref. 21, show an underprediction by the wavepacket model at the sideline.

The wavepacket model has good agreement with the data at higher frequencies. In the measured data at 250 Hz, there appears to be a double peak in the levels along plane one and two. While the single wavepacket model best fits smoothly varying data with a single Mach wave radiation, Stout et al.²⁰ showed that this double peak and the corresponding directivity could be modeled using two wavepackets. This could be the subject of future work. At 500 Hz, the ground reflection affected the wavepacket model, but the addition or removal of an image source did not significantly affect the performance of the optimization. Finally, at high frequencies (1000 Hz or more), the source region became very compact and behaved almost like a point source. Despite this compact shape, the agreement between the measured data and the optimized results were very good.

Comparisons can be made between these optimized wavepackets and the work of Stout et al.¹⁸ Using intensity vectors, Stout et al. traced the intensity vectors that were within 3 dB of the peak intensity level back to the centerline of the jet. This gives an estimated source region. Then using a simulation, Stout et al. found that this corresponded to the region of the wavepacket greater than eighty percent of the peak. Thus, in this study, the source region is defined as the portion of the wavepacket greater than eighty percent of the peak amplitude. This definition allows comparisons to be made between the two methods. Figure 6 shows the source region from Stout's ray tracing (red) compared to the wavepacket model (green). The wavepacket model predicts a more upstream position for the source region and the source region becomes quite small above 500 Hz. Nevertheless, the two methods are close if not collocated, and have similar trends for the source region. Furthermore, comparisons between the maximum and minimum direction of the acoustic intensity vectors that are within 3 dB of the peak intensity level are similar. At higher frequencies, the optimized wavepackets have a smaller source region and therefore a slightly wider angle for directivity of the intensity vectors than Stout et al. The angle of the peak acoustic intensity level can be computed from the optimized convective velocity using Eq. 2. This computed angle shown in Fig. 7 (which is the inlet angle, rather than the exhaust/centerline angle) agrees very well with both Stout et al.'s directionality and the optimized wavepacket directionality.

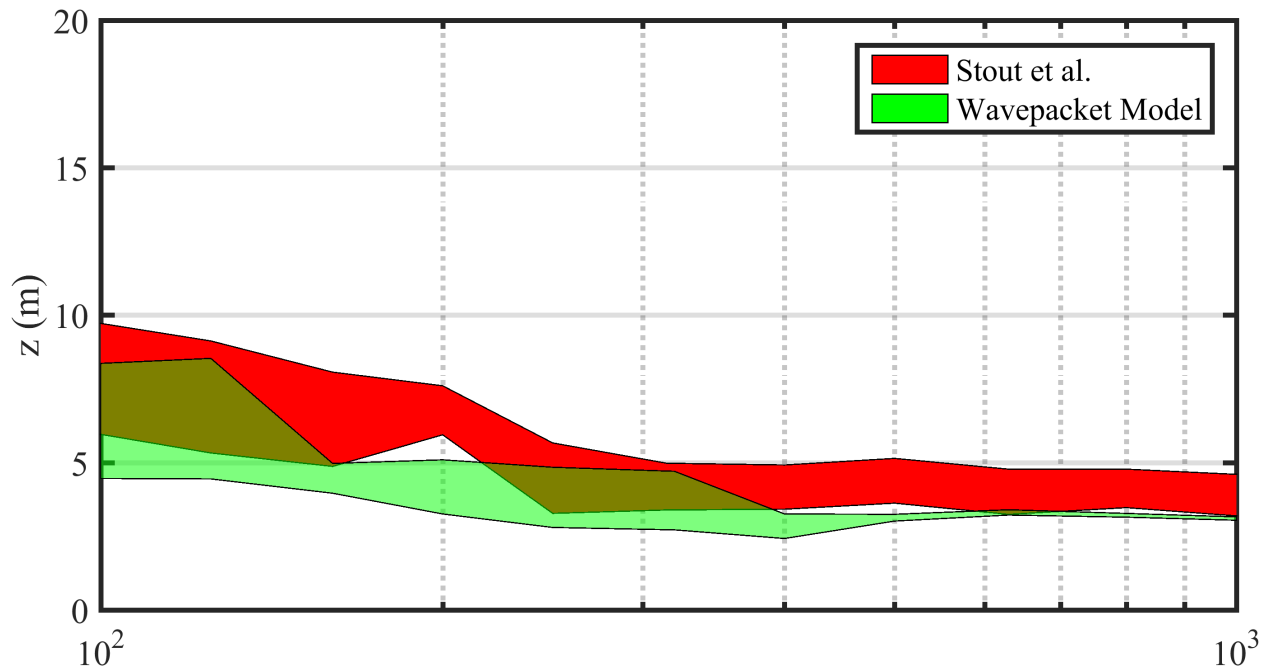


Figure 6. Comparison between Stout et al. method and the wavepacket optimized method for finding the source region at military engine conditions.

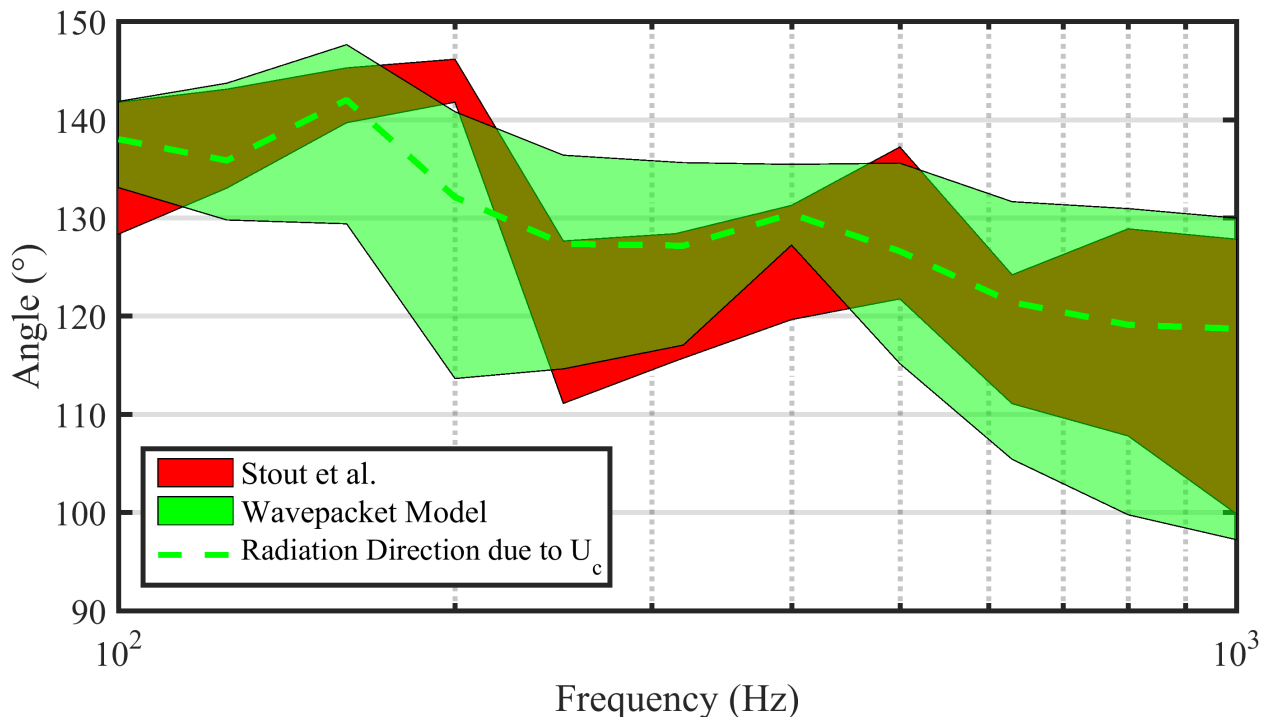


Figure 7. Comparison between Stout et al. method and the wavepacket optimized method for finding the direction of energy flow at military engine conditions. The dotted green line represents the peak radiation direction computed from the convective velocity using Eq. 2.

B. AFTERBURNER ENGINE CONDITION

Even though the measured intensity levels from afterburner engine condition were not as smooth as the military engine condition, the wavepacket model still fits the data reasonably well and agrees with the results of

Stout et al (see Fig. 8). At 100 Hz, the source region extends from about 6 m to 12 m. This is similar to Stout's source region, which extends from about 7 m to 11 m. Generally, as frequency increases, the optimized wavepacket model shows the source region as being narrower and closer to the engine nozzle. An exception is at 250 Hz, where the source region is broader. This could be the result of a double peak in the Mach wave radiation as discussed in the military engine condition. Furthermore, as expected, the source region has a linear trend for the location moving upstream, as well as a steadily decreasing spatial extent. There are some differences between the two source regions, but the general location downstream is similar for both models.

For the afterburner directionality, there is good agreement between the two methods (see Fig. 9). The two methods disagree by roughly 10 degrees between 250 and 500 Hz, but otherwise have overlapping regions. Like the military condition, because of the small source region, the directionality at higher frequencies is broader than the results by Stout et al. Lastly, as expected, the main radiation from the afterburner engine condition radiates farther upstream than the military engine condition.

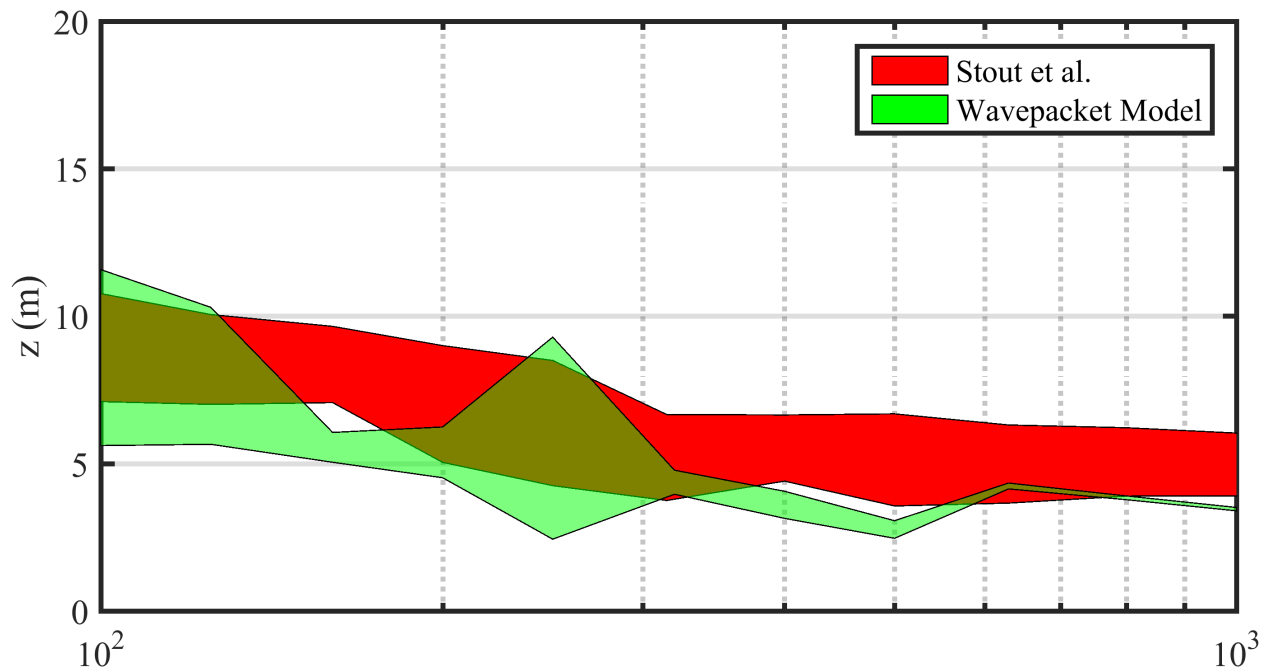


Figure 8. Comparison between Stout et al. method and the wavepacket optimized method for finding the source region at afterburner engine conditions.

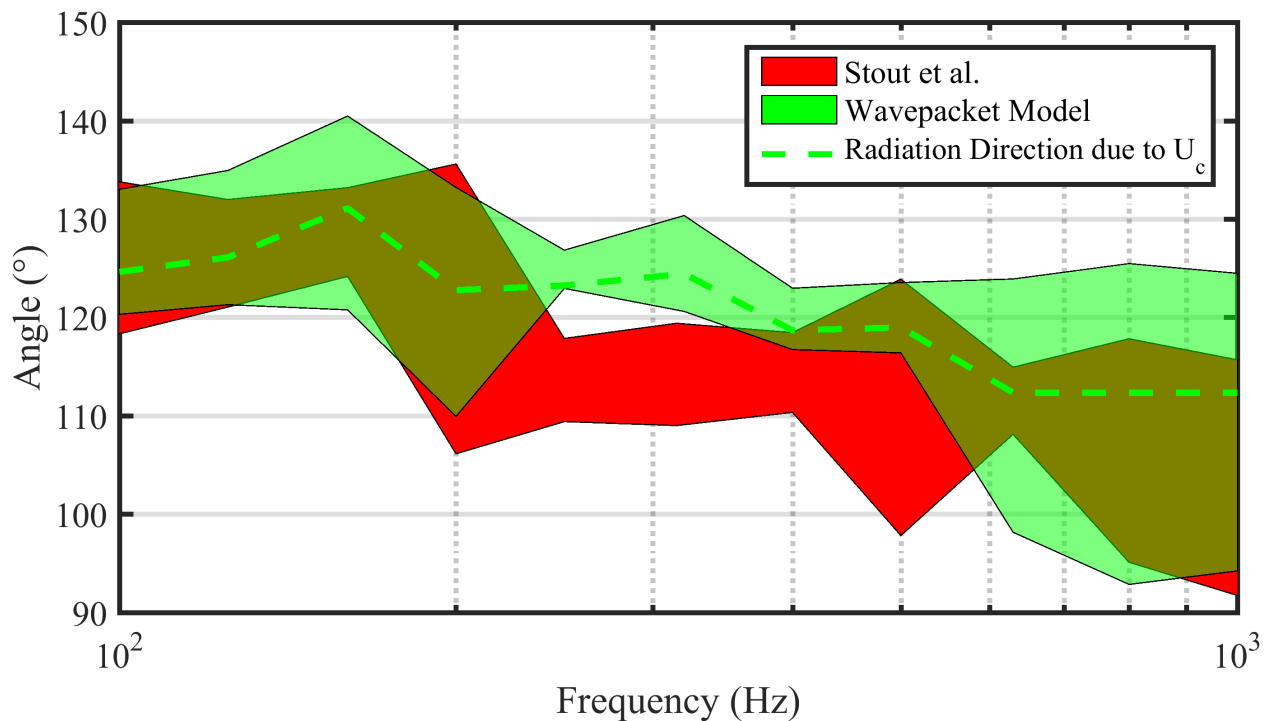


Figure 9. Comparison between Stout et al. method and the wavepacket optimized method for finding the direction of energy flow at afterburner engine conditions. The dotted green line represents the peak radiation direction computed from the convective velocity using Eq. 2.

4. CONCLUSION

Intensity-based, volume velocity (source strength) wavepackets have been obtained from the acoustic vector intensity measured by a tethered advanced tactical aircraft with one engine operating at different engine conditions. The frequency-dependent wavepackets constitute an equivalent source model that can be used to model the spatially distributed intensity field. This intensity-based equivalent noise source shows similarities to previous source characterization efforts. The equivalent source model matched the data well especially when the data was smoothly varying and had a single main radiation lobe. This is most noticeable at low frequencies around 125 Hz for both engine conditions. As a further validation of the method, the source location and directivity were correlated between Stout's ray tracing work and the wavepacket optimization method. As would be expected, in both works, the source location moves upstream and the spatial extent decreases as the frequency increases. Furthermore, although the spatial extent between the two methods varies at higher frequencies, the source region location is in a similar position. Finally, the directivity of both methods gives similar results.

The optimization modeling technique can be improved in future modeling. For one, some of the data had multiple radiation lobes, which were more difficult for the optimized single wavepacket model to fit. This could be improved, by using multiple wavepackets. In addition, this work ignored the coherence lengths characteristic of jet noise because of the sparsity of the data. Acoustic array processing of the same data indicates⁴ coherence lengths much smaller than a single wavepacket model can produce. Multiple wavepackets that incoherently add to form an equivalent single wavepacket are needed to match the measured coherence lengths. However, using the current measurement data, it is impossible to include coherence information, because the intensity measurements were not taken at the same time. In the future, the optimized wavepacket equivalent source model can be used to predict acoustic quantities away from the source without much computational expense.

ACKNOWLEDGMENTS

Most of this work was carried out under a grant from the Office of Naval Research. Distribution A. Approved for public release; distribution unlimited. 88ABW-2020-0682; cleared on 24 Feb 2020.

REFERENCES

- ¹ C. K. W. Tam, "Supersonic jet noise," *Annu. Rev. Fluid Mech.* **27**, 17-43 (1995).
- ² J. Morgan, T. B. Neilsen, K. L. Gee, A. T. Wall and M. M. James, "Simple-source model of high power jet aircraft noise", *Noise Control Engr. J.* **60** (4), 435-449, (2012).
- ³ A. T. Wall, K. L. Gee, T. B. Neilsen, R. L. McKinley, and M. M. James, "Military jet noise source imaging using multisource statistically optimized near-field acoustical holography," *J. Acoust. Soc. Am.* **139**, 1938-1950 (2016)
- ⁴ B. M. Harker, K. L. Gee, T. B. Neilsen, A. T. Wall, and M. M. James, "Wavepacket modeling and full-scale military jet noise beamforming analyses", *AIAA Paper* 2016-2129, (2016).
- ⁵ T. B. Neilsen, K. L. Gee, B. M. Harker, and M. M. James, "Level-educed Wavepackets Representation of Noise Radiation from a High-performance Military Aircraft", *AIAA Paper* 2016-1880, (2016).
- ⁶ B. M. Harker, K. L. Gee, T. B. Neilsen, A. T. Wall, and M. M. James, "Source characterization of full-scale tactical jet noise from phased-array measurements," *J. Acoust. Soc. Am.* **146**, 665-680 (2019).
- ⁷ A. T. Wall, K. L. Gee, M. M. James, K. A. Bradley, S. A. McInerny, and T. B. Neilsen, "Near-field noise measurements of a high-performance military jet aircraft", *Noise Control Engr. J.* **60** (4), 421-434, (2012).
- ⁸ P. Jordan and T. Colonius, "Wave Packets and Turbulent Jet Noise", *Annu. Rev. Fluid Mech.* **45**, 173-195, (2013).
- ⁹ T. Suzuki and T. Colonius, "Instability waves in a subsonic round jet detected using a near-field phased microphones array" *J. Fluid Mech.*, **565**, 197-226, (2006).
- ¹⁰ T. Suzuki, "Coherent noise sources of a subsonic round jet investigated using hydrodynamic and acoustic phased-microphone arrays", *J. Fluid Mech.*, **730**, 659-698, (2013).
- ¹¹ F. Kerherve, A. Guitton, P. Jordan, and J. Delville, V. Fortune, Y. Gervais, and C. Tinney, "Identifying the dynamics underlying the large-scale and fine-scale jet noise similarity spectra", *AIAA Paper* 2008-3027, (2008).
- ¹² Reba, R. J. Simonich and R. Schlinker, "Measurement of Source Wave-Packets in High-Speed Jets and Connection to Far-Field Sound," *AIAA Paper* 2008-2891, May 2008.
- ¹³ M. Koenig, A. V. G. Cavlieri, P. Jordan, J. Delville, Y. Gervais, and D. Papamoschou, "Farfield filtering and source imaging of subsonic jet noise", *J. Sound Vibr.*, **332** (18), 4067-4088, (2013).
- ¹⁴ P. J. Morris "A note on noise generation by large scale turbulent structures in subsonic and supersonic jets", *Int. J. Aeroacoust.* **8** (4), 301-315, (2009).
- ¹⁵ C. K. W. Tam, M. Golebiowski, and J. M. Seiner, "On the two components of turbulent mixing noise from supersonic jets", *AIAA Paper* 96-1716, (1996).
- ¹⁶ D. J. Roth, "Sound intensity techniques for identifying locations of scale model jet noise sources", *J. Acoust Soc. Am.* **75**, S80 (1984).
- ¹⁷ S. M. Jaeger and C. S. Allen, "Two-dimensional sound intensity analysis of jet noise", *AIAA Paper* 93-4342, (1993).
- ¹⁸ T. A. Stout, K. L. Gee, T. B. Neilsen, A. T. Wall, and M. M. James, "Source characterization of full-scale jet noise using acoustic intensity", *Noise Control Engr. J.* **63** (6), 522-536, (2015).
- ¹⁹ D. C. Thomas, B. Y. Christensen, and K. L. Gee, "Phase and amplitude gradient method for estimation of acoustic vector quantities", *J. Acoust. Soc. Am.* **137** (6), 3366-3376 (2015).
- ²⁰ T. A. Stout, K. L. Gee, T. B. Neilsen, D. W. Krueger, and M. M. James, "Intensity analysis of the dominant frequencies of military jet aircraft noise," *Proc. Mtgs. Acoust.* **20**, 040010 (2014)
- ²¹ D. Papamoschou, "Wavepacket Modeling of Jet Noise Sources," *AIAA Paper* 2011-2835, (2011).
- ²² R. Reba, S. Narayanan, and T. Colonius, "Wave-packet models for large-scale mixing noise", *Int. J. Aeroacoust.* **9**, 533-558, (2010).
- ²³ J. Reba, J. Simonich, and R. Schlinker, "Sound Radiated by Large-Scale Wave-Packets in Subsonic and Supersonic Jets", *AIAA Paper* 2009-3256, (2009).
- ²⁴ N. E. Murray and G. W. Lyons, "On the convection velocity of source events related to supersonic jet crackle," *J. Fluid Mech.* **793**, 477-503 (2016).
- ²⁵ S. Kirkpatrick, C. D. Gelatt Jr., M. P. Vecchi, "Optimization by Simulated Annealing", *Science* **220** (4598), 671-680, (1983).
- ²⁶ N. Metropolis, A. W. Rosenbluth, M. N. Rosenbluth, A. H. Teller, and E. Teller, "Equation of State Calculations by Fast Computing Machines", *J. Chem. Phys.* **21**, 1087 (1953).
- ²⁷ K. L. Gee, V. W. Sparrow, M. M. James, J. M. Downing, C. M. Hobbs, T. B. Gabrielson, and A. A. Atchley, "The role of nonlinear effects in the propagation of noise from high-power jet aircraft," *J. Acoust. Soc. Am.* **123**, 4082-4093 (2008).
- ²⁸ C. K. W. Tam, K. Viswanathan, K. K. Ahuja, and J. Panda, "The sources of jet noise: Experimental evidence," *J. Fluid Mech.* **615**, 253-292 (2008).